



Structure and composition of sputter-deposited nickel-tungsten oxide films

S.V. Green^{a,*}, A. Kuzmin^b, J. Purans^b, C.G. Granqvist^a, G.A. Niklasson^a

^a Department of Engineering Sciences, The Ångström Laboratory, Uppsala University, P.O. Box 534, SE-751 21 Uppsala, Sweden

^b Institute of Solid State Physics, University of Latvia, 8 Kengaraga Street, Riga, Latvia

ARTICLE INFO

Article history:

Received 6 May 2010

Received in revised form 8 October 2010

Accepted 12 October 2010

Available online 21 October 2010

Keywords:

Tungsten oxide

Nickel oxide

X-ray photoelectron spectroscopy

Rutherford backscattering

X-ray diffraction

Raman spectroscopy

ABSTRACT

Films of mixed nickel-tungsten oxide, denoted $\text{Ni}_x\text{W}_{1-x}$ oxide, were prepared by reactive DC magnetron co-sputtering from metallic targets and were characterized by Rutherford backscattering spectrometry, X-ray photoelectron spectroscopy, X-ray diffractometry and Raman spectroscopy. A consistent picture of the structure and composition emerged, and at $x < 0.50$ the films comprised a mixture of amorphous WO_3 and nanosized NiWO_4 , at $x = 0.50$ the nanosized NiWO_4 phase was dominating, and at $x > 0.50$ the films contained nanosized NiO and NiWO_4 .

© 2010 Elsevier B.V. All rights reserved.

1. Introduction

Films of tungsten oxide and nickel oxide have many applications, such as in electrochromic devices, gas sensors and photocatalytic surfaces [1,2]. Mixed nickel-tungsten oxide films, denoted $\text{Ni}_x\text{W}_{1-x}$ oxide, may have properties that are superior to those of the two components. In this work $\text{Ni}_x\text{W}_{1-x}$ oxide films were investigated with the main objective to elucidate the structural evolution of the phases that emerge for $0 < x < 1$.

Our specific interest is connected with the electrochromic properties of the $\text{Ni}_x\text{W}_{1-x}$ oxide system. Electrochromic materials change their optical properties when a potential is applied so that electrical charge is inserted or extracted. Both tungsten oxide and nickel oxide are widely used materials with excellent and complementary electrochromic properties [1–3]. The electrochromic effect ensues from electron transitions between different atomic states. For tungsten oxide, electron transitions between W^{5+} and W^{6+} cause absorption which sets in progressively as the W^{5+} content is increased. Nickel oxides with Ni^{2+} are transparent, which is the case for NiO and/or $\text{Ni}(\text{OH})_2$, whereas oxides with Ni^{3+} are absorbing and this is so for NiOOH and/or Ni_2O_3 .

Mixed oxide thin films can have improved electrochromic properties, as has been known for many years [2,4–7], and at least one study has been made on thin film electrochromic tungsten oxide containing nickel, showing that the additive had beneficial effects that led to faster response times for the optical modulation, lower power consumption and good stability [8]. There is also some prior work by Kuzmin et al. on

thin films of nickel tungstate, NiWO_4 , with foci on local atomic structure and electrochromic properties [9,10].

The phase diagram for the bulk $\text{NiO}-\text{WO}_3$ system forms a suitable point of departure for discussing thin films of this material. The system does not form solid solutions and the only compound NiWO_4 melts incongruently at 1420 °C and forms a eutectic with WO_3 at 73 mol % WO_3 and 1245 °C [11]. The crystalline phases present after solidification of melts are comprised of $\text{NiO} + \text{NiWO}_4$ and $\text{NiWO}_4 + \text{WO}_3$ in the composition range below and above 50 mol % WO_3 , respectively. These results may provide guidelines for structural evolutions, but films of $\text{Ni}_x\text{W}_{1-x}$ oxide can sustain metastable phases so that structural and compositional characterizations are essential in order to develop a fundamental understanding of their properties, notably for the electrochromic performance. To that end we studied sputter-deposited $\text{Ni}_x\text{W}_{1-x}$ oxide films with several different techniques, specifically being Rutherford backscattering spectrometry (RBS), X-ray photoelectron spectroscopy (XPS), X-ray diffractometry (XRD), and Raman spectroscopy (RS).

The present work forms part of a larger investigation of the electrochromic films of $\text{Ni}_x\text{W}_{1-x}$ oxide. As a starting point for this investigation, we reported recently on the electrochromism of pure tungsten oxide and nickel oxide in various electrolytes [12].

2. Sample preparation and characterization techniques

Mixed nickel-tungsten oxide thin films were made by reactive DC magnetron co-sputtering from separate 5-cm-diameter metallic targets of pure tungsten and pure nickel in a versatile deposition system based on a Balzer UTT 400 unit. Depositions took place in a gas mixture with an O_2/Ar mass flow ratio of 0.15 and a working pressure

* Corresponding author. Tel.: +46 18 471 3129; fax: +46 18 471 3270.
E-mail address: sara.green@angstrom.uu.se (S.V. Green).

of ~ 4 Pa. A comparison with the voltages for sputtering from pure Ni and W targets indicates that the co-sputtering was carried out in the reactive mode. The target–substrate separation was ~ 13 cm. The total discharge power, $P_W + P_{Ni}$, was set to 230 W. The power to the targets was varied in order to obtain Ni_xW_{1-x} oxide thin films with different magnitudes of x . Some samples were deposited onto unheated 5×5 cm² glass plates precoated with transparent and electron conductive $In_2O_3:Sn$ in order to allow electrochemical measurements for subsequent investigation of the electrochromic properties. The XPS measurements used small pieces of such films. XRD, RBS and RS measurements were made on films deposited onto Si, C and pure glass, respectively. Some samples on silicon substrates were post-treated at 800 °C for 6.5 h in air in order to induce crystallization. Film thicknesses, as measured by an Alpha step profilometer, were 200 to 300 nm except for some RS samples that were as thick as 1 μ m in order to ensure good Raman signals.

RBS gave information on composition and density for the whole film–substrate system when data were fitted to a model by use of the SIMNRA code [13]. The spectra reveal what kind of atom is detected (by peak position), atomic concentration (by relative peak height), and thickness in atoms/cm² (by peak width). These measurements were carried out at the Uppsala Tandem Laboratory using 2 MeV ⁴He ions backscattered at an angle of 172°.

XPS measurements were performed with a PHI Quantum 2000 Scanning ESCA Microprobe operating with monochromated AlK_{α} radiation (1486 eV), a pass energy of 46.95 eV and a step size of 0.2 eV/s. Energy calibration was done by setting the binding energy of C 1s to 284.5 eV. Spectra were analysed using the Multipak program [14] and the magnitude of x was obtained from integration over the W 4f and Ni 2p peaks.

XRD information was recorded on a Siemens D5000 diffractometer operating with CuK_{α} radiation at a wavelength of 1.54 Å. The detector was a parallel plate collimator with an acceptance angle of 0.4°. During measurements the incoming beam was fixed at an angle of 1°, and the detector angle was scanned with 2 s/step for increments of 0.05°. Structure, phase composition and orientation of the planes were inferred by comparing experimental spectra with the JCPDS database.

RS data were taken at room temperature (20 °C) by use of a confocal microscope with a “Nanofinder-S” (SOLAR TII, Ltd.) spectrometer [15]. The measurements were performed through a Nikon CF Plan Apo 100 \times (NA = 0.95) optical objective. The Raman spectra were excited with a He–Cd laser (441.6 nm, 50 mW cw power) and dispersed by a 600 grooves/mm diffraction grating mounted in a 520 mm focal length monochromator. To exclude possible sample heating, the laser power at the sample was regulated by a variable neutral-density filter (optical density from zero to 3.1). A Peltier-cooled back-thinned CCD camera (ProScan HS-101H, 1024 \times 58 pixels) was used as the detector. The elastic laser light component was eliminated by an edge filter (Omega, 441.6AELP-GP).

3. Results and discussion

3.1. Composition found by RBS and XPS

The composition dependence of the Ni_xW_{1-x} oxide thin films on the sputter power ratio P_{Ni}/P_W was readily inferred from RBS and XPS as shown in Fig. 1. The RBS and XPS values from the two sets of measurements were in good agreement. The figure also illustrates whether the samples were visually transparent or not. The colour of the dark films was brownish. The reason for the sudden increase in x when P_{Ni}/P_W is 1.9 is not known, but it seems that whether films deposited in this range are transparent or absorbing is very sensitively dependent on the detailed sputtering conditions [16]. The density, found by RBS, lay close to that of W oxide films, i.e. in the 5 to 6 g/cm³ range [2,12].

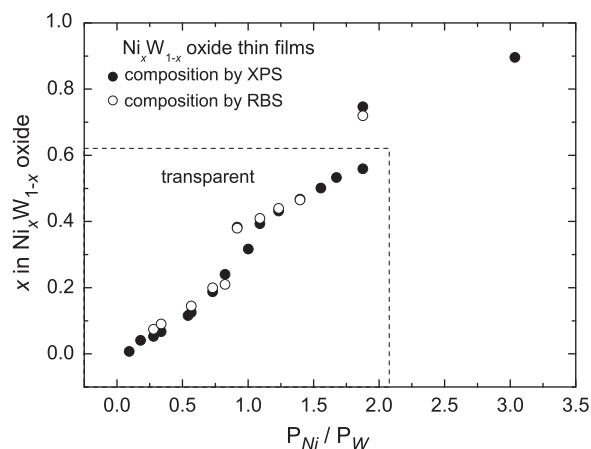


Fig. 1. Composition of Ni_xW_{1-x} oxide thin films as determined by two techniques vs ratio of sputter powers, and visual impression.

3.2. W 4f, Ni 2p and O 1s binding energies analysed by XPS

XPS is a surface sensitive technique whose depth sensitivity is limited by the mean-free path of the escaping electron to about 10 to 100 Å. A rigorous treatment of the XPS spectra in transition metal oxides requires an account for many-body charge-transfer effects, which are responsible for a characteristic splitting of the 2p spectra of transition metal compounds [17]. In the present work, we will limit our analysis of the Ni 2p, W 4f and O 1s XPS spectra to the estimation of binding energies and peak intensities, which will be used to evaluate the oxidation state of metal ions and the film compositions. A comparison with known XPS data will be given for several reference compounds.

3.2.1. W 4f

In pure tungsten oxide, i.e. $W^{6+}O_3$, the W 4f_{7/2} and W 4f_{5/2} peaks lie at 35.6 and 37.7 eV, respectively [18,19]. The positions of the two peaks for W^{5+} are located at lower binding energies, specifically at 34.9 and 37.1 eV [19]. Even smaller binding energies, at 33.5 and 35.8 eV, are expected for W^{4+} [19]. The binding energy for W 4f_{7/2} in $NiWO_4$ has been found to lie at 35.4 [18] and 35.2 eV [20], i.e. close to that of W^{6+} .

Fig. 2 shows that the W 4f spectra in our films consist of well-resolved spin orbit split doublet peaks corresponding to W 4f_{7/2} and W 4f_{5/2} states. For the pure W oxide film the locations of the two peaks suggest a W^{6+} state. No change, as compared to the case of pure transparent W oxide, was found for films with Ni contents up

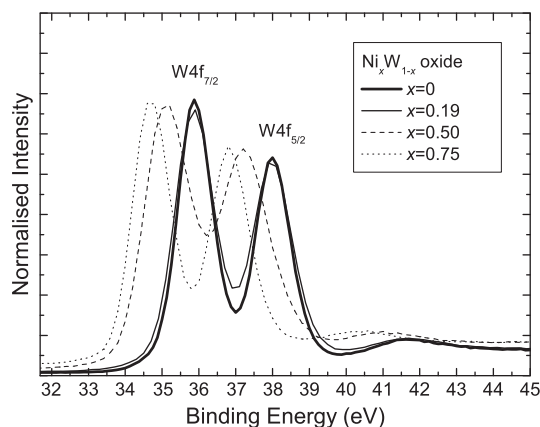


Fig. 2. W 4f XPS spectra for pure W oxide and mixed Ni_xW_{1-x} oxide films. The small peak at 41 to 42 eV is due to W 5p_{3/2}.

to $x \approx 0.20$. Upon addition of up to $x = 0.5$, the binding energies of W $4f_{7/2}$ and W $4f_{5/2}$ states decreased slightly and some peak broadening was observed. As even more Ni was added, a film with $x = 0.75$ became dark in colour and the double peak changed to lower binding energies, as shown in Fig. 2. This peak shift is due to the presence of reduced tungsten ions W^{5+} [2,19]. For $x = 0.50$ the peak is displaced to a binding energy close to that of $NiWO_4$, but the shift for the dark $Ni_{0.75}W_{0.25}$ oxide could also be due to the presence of W^{5+} . Also the broadening of the peak for $Ni_{0.50}W_{0.50}$ oxide could be associated with W^{5+} .

3.2.2. Ni 2p

For nickel oxides the Ni 2p spectra contain multiple peaks at binding energies between about 852 and 870 eV, including the main peak and satellites [21–23]. According to theory for the XPS technique [24–26], these peaks have been interpreted as due to final state effects caused by charge transfer from oxygen to nickel. The Ni $2p_{3/2}$ XPS spectra in $Ni(OH)_2$ and $NiOOH$ [22] have more broadened shapes than in NiO, and the first peak for $NiOOH$ is shifted to larger binding energies thereby reflecting the presence of Ni^{3+} . As mentioned, the Ni 2p spectra are often complex and contain multiple peaks, and it is difficult to assign specific binding energies to the Ni^{2+} and Ni^{3+} states. For example, a recent work put the main peaks for NiO, $Ni(OH)_2$ and $NiOOH$ at 854.7, 855.3 and 855.8 eV, respectively [22]. The main peak due to Ni $2p_{3/2}$ in $NiWO_4$ was reported to lie at 857.7 [18], 857.5 [20] and 856.2 eV [27].

Fig. 3 presents XPS spectra for the Ni $2p_{3/2}$ peak. They consist of two broad bands located at 853 to 858 eV and 860 to 866 eV. For $x \leq 0.5$ the positions of the main peak and of the satellite are found at about 856.5 and 863 eV, respectively; these values are close to the binding energy of nickel in $NiWO_4$. The main peak is progressively shifted to lower binding energies for higher nickel content, i.e. for $x > 0.5$. At $x = 0.75$ the binding energy of the main peak is decreased by about 1 eV, down to ~ 855.5 eV. This decrease can be explained by the appearance of a NiO phase in films with $x > 0.5$. However one cannot exclude the presence of $NiOOH$, since the sample has a darkish brown colour that indicates the presence of some Ni^{3+} , which possibly is responsible for the asymmetry of the XPS peaks.

3.2.3. O 1s

The O 1s binding energy of $NiOOH$ is 531.7 eV [28], while the corresponding energies are 529.6, 531.3 and 531.8 eV for NiO, $Ni(OH)_2$ and Ni_2O_3 , respectively [18]. The O 1s binding energy for crystalline $NiWO_4$ lies at 531.5 eV [20] and for WO_3 at 530.6 eV [18].

Fig. 4 shows the O 1s peak for pure W oxide and mixed Ni_xW_{1-x} oxide films with different amounts of Ni. The peak at 530.8 eV for pure WO_3 is in close agreement with literature data [18,20,29,30]. An addition of Ni makes the peak widen and shift. It has been shown [31]

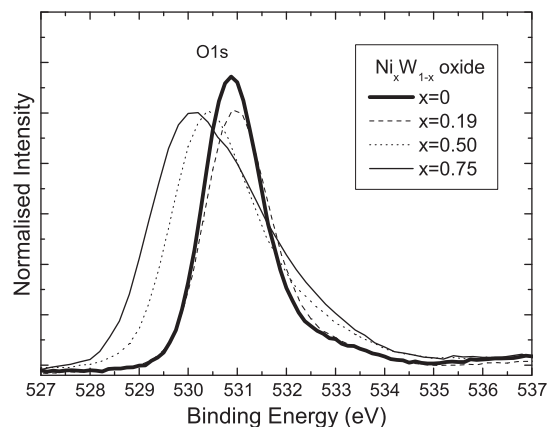


Fig. 4. O 1s XPS spectra for pure W oxide and mixed Ni_xW_{1-x} oxide films.

that the O 1s peak in W oxide is not affected by stoichiometry, i.e. the observed changes of the peak should be solely the result of the presence of another phase, caused by nickel ions. For $x = 0.5$ the O 1s peak shifts to 530.4 eV, indicating the presence of nanosized $NiWO_4$. It is expected that a local structure relaxation in nano- $NiWO_4$ will slightly decrease the O 1s binding energy compared to that of crystalline $NiWO_4$. Moreover the phases with larger O 1s binding energies, such as $Ni(OH)_2$, $NiOOH$ and Ni_2O_3 , could contribute to the high-energy tail. The larger shift towards lower binding energies, seen for Ni-rich films with $x \geq 0.50$, can be related to the appearance of a nickel oxide phase in which oxygen atoms have lower binding energy. The colour of the film with $x = 0.75$ and the broadening of the peak towards higher binding energies could also indicate that some Ni^{3+} -containing phase is present.

3.3. Structures determined by XRD

As-deposited pure W oxide and mixed Ni_xW_{1-x} oxide films were found to be X-ray amorphous up to $x = 0.75$. They become crystalline upon high-temperature treatment at 800 °C.

Fig. 5 shows results for annealed pure W oxide and a mixed Ni_xW_{1-x} oxide film with $x = 0.5$. Both samples have a monoclinic structure and the peaks agree with literature data for WO_3 [32] and $NiWO_4$ [33], respectively. Fig. 6 shows results for an as-deposited polycrystalline Ni oxide film and for annealed mixed Ni_xW_{1-x} oxide with $x = 0.75$. The latter film consists primarily of a cubic rock-salt NiO phase [34], but there is some evidence, shown by the peaks marked with asterisks, that $NiWO_4$ is present: this assignment can be made by comparison with the data in Fig. 5. Our XRD results on annealed thin films are in full agreement with the phase diagram of the bulk NiO– WO_3 system [11].

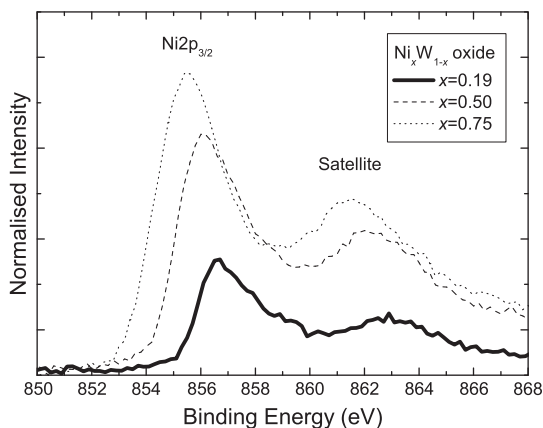


Fig. 3. Ni $2p_{3/2}$ XPS spectra for mixed Ni_xW_{1-x} oxide films.

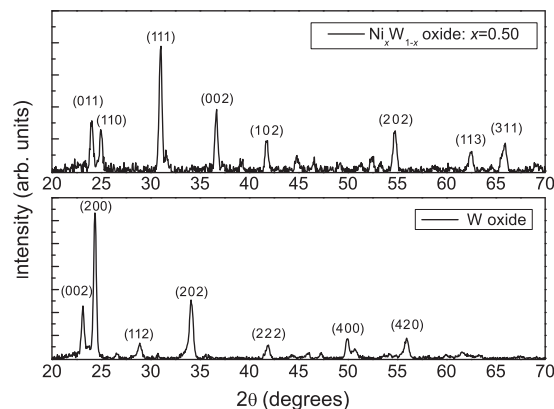


Fig. 5. XRD patterns for annealed films of $Ni_{0.5}W_{0.5}$ oxide (top) and pure W oxide (bottom). (hkl) parameters refer to the monoclinic phases of $NiWO_4$ and WO_3 .

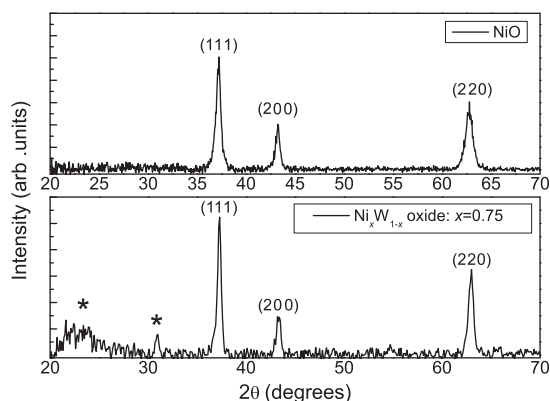


Fig. 6. XRD patterns for an as-deposited film of NiO (top) and an annealed $\text{Ni}_{0.75}\text{W}_{0.25}$ oxide film (bottom). ($h\ k\ l$) parameters refer to the cubic rock-salt structure of NiO. Peaks marked by asterisks are tentatively attributed to NiWO_4 .

3.4. Lattice dynamics probed by Raman spectroscopy

Raman spectroscopy was used to study the local dynamics in $\text{Ni}_x\text{W}_{1-x}$ oxide films with $x < 0.45$. As-deposited films were X-ray amorphous; however their local structure, and thus the local phonon modes observed by RS, can resemble those of corresponding amorphous/nanocrystalline phases of WO_3 , NiWO_4 and NiO.

Fig. 7 shows typical Raman spectra for thin films of several compositions. The spectra are dominated by two bands, located at about 790 and at 950 to 970 cm^{-1} , whose ratio changes with composition. These two bands are commonly assigned to O–W–O bond stretching and to terminal W=O modes. The Raman signal of the pure tungsten oxide corresponds to that of an amorphous film [35–37]. Upon an increase of the nickel content, the intensity of the band at 950 cm^{-1} grew and became dominant for $x > 0.2$.

An addition of nickel makes it possible to form local environments similar to those in NiWO_4 and NiO. Nickel oxide with a rock-salt structure has weak Raman scattering and normally shows a first-order defect-induced broad band at about 500 cm^{-1} [37] or a set of second-order Raman bands with the highest one at $\sim 1100\text{ cm}^{-1}$ [38] neither

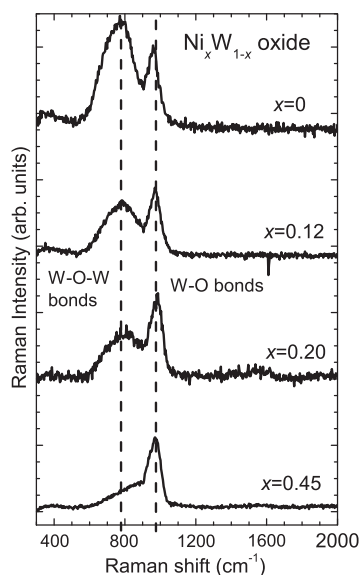


Fig. 7. Room temperature Raman spectra of pure W oxide and mixed $\text{Ni}_x\text{W}_{1-x}$ oxide films with different magnitudes of x . Vertical lines indicate the positions of the two main bands at about 790 and 970 cm^{-1} .

of which were observed in the spectra in Fig. 7. Therefore we can exclude the presence of a NiO phase in the mixed films with $x \leq 0.45$. On the other hand NiWO_4 has a very strong Raman signal and is easily detected in thin films [15]. This signal is dominated by the 891 cm^{-1} mode, which is typical for tungstates and corresponds to stretching vibration of the W–O pair in the WO_6 group, a so-called “internal” mode [39]. This band is also not present in the spectra in Fig. 7; this excludes the presence of a crystalline NiWO_4 phase, which is consistent with our XRD results.

However, it was found recently [40] that nanosized tungstates, with crystallite sizes below 2 nm, are X-ray amorphous and have a Raman signal very close to that observed in Fig. 7 for $x = 0.45$, i.e. a dominating band located at 970 cm^{-1} and a broad low-intensity band at 790 cm^{-1} . Therefore we conclude that the $\text{Ni}_x\text{W}_{1-x}$ oxide film with $x = 0.45$ has a nanosized NiWO_4 phase, which transfers into crystalline NiWO_4 upon annealing at a high temperature.

Finally, Raman signals for intermediate compositions with $0 < x < 0.45$ were found to correspond well to a weighted sum of pure amorphous W oxide and nanosized NiWO_4 phases, as shown in Fig. 8. One can utilize this result to estimate the film composition and to compare it with the nominal nickel content. At a nominal $x = 0.12$, for example, the nickel content in the film, estimated from the decomposition of the Raman signal, is about $0.24 \times 0.45 = 0.11$.

4. Conclusion

Films of mixed $\text{Ni}_x\text{W}_{1-x}$ oxide were characterized by four different techniques, specifically being RBS, XPS, XRD and RS. From RBS analysis we inferred that the density was close to that of pure W oxide films, i.e. 5 to 6 g/cm^3 . RBS together with XPS gave consistent results for the magnitude of x .

For films with $x < 0.5$, XPS and RS showed clear evidence for a thin film structure of nanosized NiWO_4 and WO_y with y close to 3. The two phases are X-ray amorphous. For $x = 0.5$, both XPS and RS show that the main constituent is nanosized NiWO_4 .

In films with $x > 0.5$, XPS gave evidence for NiO and reduced tungsten ions (W^{5+}). The tail in the O 1s spectrum at energies above 532 eV also indicated the existence of hydrated phases for $x \geq 0.5$ which, however, are difficult to identify. No clear evidence was found for NiOOH and Ni(OH)_2 , although they are often present in sputter-deposited films together with NiO [23]. In addition, the dark brownish colour of films with $x > 0.5$ indicated the presence of Ni^{3+} . No clear evidence was found for NiWO_4 by XPS, but the broadening of both the Ni 2p and O 1s peaks, in addition to the shift in the W 4f peak, could be signs of its presence.

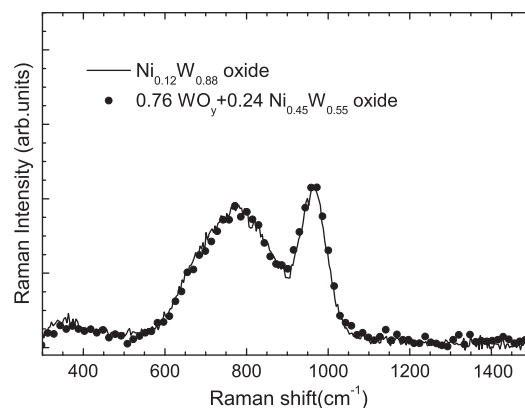


Fig. 8. Raman spectra for a mixed $\text{Ni}_x\text{W}_{1-x}$ oxide film with $x = 0.12$ (solid curve) and for a model (dots) corresponding to a weighted sum of two Raman signals: 76% of pure W oxide and 24% of $\text{Ni}_x\text{W}_{1-x}$ oxide with $x = 0.45$.

Table 1

Summary of structural phases found in sputter-deposited $\text{Ni}_x\text{W}_{1-x}$ oxide films and of the experimental techniques used to obtain this information. XPS, RS and XRD denote X-ray photoelectron spectroscopy, Raman spectroscopy and X-ray diffractometry, respectively.

x in $\text{Ni}_x\text{W}_{1-x}$ oxide	Phase	Experimental technique
$x < 0.50$	Amorphous WO_3	XPS (W 4f, O 1s), RS
	Nanosized NiWO_4	XPS (Ni 2p, O 1s), RS
$x = 0.50$	Nanosized NiWO_4	XPS (W 4f, Ni 2p), RS, XRD
	other	XPS (O 1s)
$x > 0.50$	NiO	XPS (O 1s, Ni 2p), XRD
	other	XPS (O 1s, Ni 2p)
	W^{5+} -phase	XPS (W 4f)
	Nanosized NiWO_4	XRD

The as-deposited films were X-ray amorphous for $x \leq 0.75$, but XRD on annealed samples showed that the $\text{Ni}_{0.5}\text{W}_{0.5}$ oxide film forms NiWO_4 and that the $\text{Ni}_{0.75}\text{W}_{0.25}$ oxide film forms a mixture of NiO and NiWO_4 . These results are in agreement with the phase diagram for NiO-WO_3 [11].

Finally, our analysis has given a consistent picture for the structure of the notoriously difficult $\text{Ni}_x\text{W}_{1-x}$ oxide thin films, as summarised in Table 1. This information is useful for a number of applications including electrochromics (as will be elaborated in a later paper), conductometric gas sensors, photocatalysts, and others.

Acknowledgments

This work was supported by Clear-up (Clean and Resource Efficient Buildings for Real Life) which is an Integrated Project funded by the European Community's Seventh Framework Programme (FP7/2007–2013) under grant agreement number 211948. Additional support was received from the Swedish Research Council for Environment, Agriculture Sciences and Spatial Planning (FORMAS) and by a scholarship from the Anna-Maria Lundin foundation. We are grateful to Jens Jensen for valuable input regarding RBS measurements. A. Kuzmin acknowledges the funding support from ESF Project 2009/0202/1DP/1.1.1.2.0/09/APIA/VIAA/141.

References

- [1] G.B. Smith, C.G. Granqvist, *Green Nanotechnology: Solutions for Sustainability and Energy in the Built Environment*, CRC Press, Boca Raton, FL, USA, 2010, to be published.
- [2] C.G. Granqvist, *Handbook of Inorganic Electrochromic Materials*, Elsevier, Amsterdam, The Netherlands, 1995.
- [3] G.A. Niklasson, C.G. Granqvist, *J. Mater. Chem.* 17 (2007) 127.
- [4] B.W. Faughnan, R.S. Crandall, *Appl. Phys. Lett.* 31 (1977) 834.
- [5] S. Sato, Y. Seino, *Trans. Inst. Electr. Commun. Engr. Jpn* 65-C (1982) 629.
- [6] S. Yamada, M. Kitao, in: C.M. Lampert, C.G. Granqvist (Eds.), *Large-area Chromogenics: Materials and Devices for Transmittance Control*, SPIE—The International Society for Optical Engineering, Bellingham, WA, USA, 1990, p. 246.
- [7] E. Avendaño, A. Azens, G.A. Niklasson, C.G. Granqvist, *Sol. Energy Mater. Sol. Cells* 84 (2004) 337.
- [8] P.K. Shen, J. Syed-Bokhari, A.C.C. Tseung, *J. Electrochem. Soc.* 138 (1991) 2778.
- [9] A. Kuzmin, J. Purans, R. Kalendarev, D. Pailharey, Y. Mathey, *Electrochim. Acta* 46 (2001) 2233.
- [10] A. Kuzmin, J. Purans, R. Kalendarev, *Ferroelectrics* 258 (2001) 21.
- [11] L. Weber, U. Egli, *J. Mater. Sci.* 12 (1977) 1981.
- [12] S. Green, J. Backholm, P. Georén, C.G. Granqvist, G.A. Niklasson, *Sol. Energy Mater. Sol. Cells* 93 (2009) 2050.
- [13] M. Mayer, SIMNRA: a simulation program for the analysis of NRA, RBS and ERDA, *AIP Conf. Proc.* 475 (1999) 541.
- [14] MultiPak Software Release Notes Version 6.1A, Physical Electronics, Inc, Eden Prairie, MN, USA, 1999.
- [15] A. Kuzmin, R. Kalendarev, A. Kursitis, J. Purans, *J. Non-Cryst. Solids* 353 (2007) 1840.
- [16] E. Avendaño, A. Azens, J. Isidorsson, R. Karmhag, G.A. Niklasson, C.G. Granqvist, *Solid State Ionics* 165 (2003) 169.
- [17] F. de Groot, A. Kotani, *Core Level Spectroscopy of Solids*, CRC Press, Boca Raton, FL, USA, 2008.
- [18] J.F. Moulder, W.F. Stickle, P.E. Sobol, *Handbook of X-ray Photoelectron Spectroscopy*, Physical Electronics Inc., MN, USA, 1995.
- [19] J. Zhang, J.P. Tu, X.H. Xia, Y. Qiao, Y. Lu, *Sol. Energy Mater. Sol. Cells* 93 (2009) 1840.
- [20] K.T. Ng, D.M. Hercules, *J. Phys. Chem.* 80 (1976) 2094.
- [21] S. Uhlenbrock, C. Scharfschwerdt, M. Neumann, G. Illing, H.J. Freund, *J. Phys. Condens. Matter* 4 (1992) 7973.
- [22] A.P. Grosvenor, M.C. Biesinger, R.S.C. Smart, N.S. McIntyre, *Surf. Sci.* 600 (2006) 1771.
- [23] E. Avendaño, H. Rensmo, A. Azens, A. Sandell, G. de M. Azevedo, H. Siegbahn, G.A. Niklasson, C.G. Granqvist, *J. Electrochem. Soc.* 156 (2009), P132.
- [24] G. van der Laan, J. Zaanen, G.A. Sawatzky, R. Karnatak, J.M. Esteve, *Phys. Rev. B* 33 (1986) 4253.
- [25] J. van Elp, H. Eskes, P. Kuiper, G.A. Sawatzky, *Phys. Rev. B* 45 (1992) 1612.
- [26] A. Fujimori, F. Minami, *Phys. Rev. B* 30 (1984) 957.
- [27] M.N. Mancheva, R.S. Iordanova, D.G. Klissurski, G.T. Tyuliev, B.N. Kunev, *J. Phys. Chem.* 111 (2007) 1101.
- [28] A.N. Mansour, C.A. Melendres, *Surf. Sci. Spectra* 3 (1994) 2718.
- [29] V.I. Nefedov, Y.V. Salyn, G. Leonhardt, R. Scheibe, *J. Electron. Spectrosc. Relat. Phenom.* 10 (1977) 121.
- [30] W. Lisowski, A.H.J. van den Berg, G.A.M. Kip, L.J. Hanekamp, *Fresenius J. Anal. Chem.* 341 (1991) 196.
- [31] O. Yu. Khyzhun, *J. Alloys Compd.* 305 (2000) 1.
- [32] Joint Committee on Powder Diffraction Standards — International Centre for Diffraction Data, card number: 83-0950.
- [33] Joint Committee on Powder Diffraction Standards — International Centre for Diffraction Data, card number: 15-0755.
- [34] Joint Committee on Powder Diffraction Standards — International Centre for Diffraction Data, card number: 78-0429.
- [35] J.V. Gabrusenoks, P.D. Cizmach, A.R. Lusi, J.J. Kleperis, G.M. Ramans, *Solid State Ionics* 14 (1984) 25.
- [36] M.F. Daniel, B. Desbat, J.C. Lassegues, B. Gerand, M. Figlarz, *J. Solid State Chem.* 67 (1987) 235.
- [37] S.H. Lee, H.M. Cheong, J.G. Zhang, A. Mascarenhas, D.K. Benson, S.K. Deb, *Appl. Phys. Lett.* 74 (1999) 242.
- [38] E. Cazzanelli, A. Kuzmin, G. Mariotto, N. Mironova-Ulman, *J. Phys. Cond. Matter* 15 (2003) 2045.
- [39] Y. Liu, H. Wang, G. Chen, Y.D. Zhou, B.Y. Gu, B.Q. Hu, *J. Appl. Phys.* 64 (1988) 4651.
- [40] A. Kalinko, A. Kuzmin, *J. Lumin.* 129 (2009) 1144.